Taylor & Francis
Taylor & Francis Group

Advanced Composite Materials

ISSN: 0924-3046 (Print) 1568-5519 (Online) Journal homepage: http://www.tandfonline.com/loi/tacm20

Lightweight fiber-reinforced plastic constructions using improved overlap forms

Guang-Min Luo & Chia-Wen Wu

To cite this article: Guang-Min Luo & Chia-Wen Wu (2015) Lightweight fiber-reinforced plastic constructions using improved overlap forms, Advanced Composite Materials, 24:6, 545-560, DOI: 10.1080/09243046.2014.937137

To link to this article: http://dx.doi.org/10.1080/09243046.2014.937137

Advanced Composite Materials, 2015
Vol. 24, No. 6, 545–560, http://dx.doi.org/10.1080/09243046.2014.937137

Lightweight fiber-reinforced plastic constructions using improved overlap forms

Guang-Min Luo* and Chia-Wen Wu

Department of Naval Architecture and Ocean Engineering, National Kaohsiung Marine University, No.142, Haijhuan Rd., Nanzih Dist., Kaohsiung City 81157, Taiwan (R.O.C.)

(*Received 8 February 2014; accepted 18 June 2014*)

Fiber-reinforced plastic (FRP) has been used to construct various vehicle forms because its lightweight properties facilitate motion and operation. Such lightweight structures can both provide sufficient strength and save material cost. Because fiber cloth is limited by its dimensions, an overlap installation is required to ensure its structural strength; however, overlap installation increases structural weight by approximately 10–15%. In this study, experiments and numerical simulations were conducted to compare the mechanical properties of various overlap forms. Based on the findings, a laminated FRP stacking arrangement is proposed for use in vehicle structures. The 'full overlap (FO)' method is traditionally used to maintain the continuity of FRP structures; however, this study explored the 'full butt' and 'outer layer for overlap and inner layer for butted-joint (OOAIB)' methods. In order to simulate the structural discontinuity at overlap region and butted-joint region, a new approach to establish finite element model is presented in this paper. According to experimental and simulated results, FO and OOAIB are similar regarding strength and stiffness. Therefore, the OOAIB method is suggested for decreasing the weight of FRP structure.

Keywords: FRP; numerical simulation; overlap; butt joint

1. Introduction

Because the length of fiber cloth is limited, large-scale laminated fiber-reinforced plastic (FRP) constructions, such as wind-power blades and FRP yachts, are required to ensure the continuity of overlap installations during stacking procedures. Ensuring sufficient strength warrants using overlap installations because of the discontinuous fiber cloth used in the stacking layers; this is referred to as the full overlap (FO) method. The overlapped zones generate an additional design weight of approximately 10–15%. Thus, this study explored enhancing overlap forms to decrease the weights of laminated constructions.

This study also examined the 'full butt (FB)' and 'outer layer for overlap and inner layer for butted-joint (OOAIB)' methods. Because the adjacent layers near the butt joint are continuous, it is assumed that the loading communication is delivered by the adjacent layers. However, FB samples demonstrate insufficient loading communication between two outer layers. The OOAIB form was developed to improve this situation.

*Corresponding author. Email: gmluo@webmail.nkmu.edu.tw

Various related studies have been recently conducted. The reports of Beylergil et al. [1] and Langella et al. [2] clearly indicated that the overlap region affects the strengths of laminated constructions. The overlap length of each stacking layer is conservatively determined to ensure sufficient strength in the overlap region; hence, the actual weights of laminated structure are heavier compared with the designed weights. Blom et al. [3] addressed the relations among overlap stacking thickness and strength; if the mechanical properties of overlap forms are known, the overlap forms can be adjusted to achieve a lightweight design.

When overlap installations are used to connect two components, adsorption occurs in the resin between adjacent layers. Delale et al. [4] used numerical analysis to confirm the continuity properties among discontinuous zones. Assessing the discontinuity of the overlap enables determining the stress concentration at the tip of overlap region when loading or bending moment occurs.[5] Agarwal and Broutman [6] examined varying fracture modes of the stress concentrations caused by overlap namely, delamination, separation between the fiber and matrix, and transverse matrix fractures at the overlap region.

Experimental method has been widely used for discussing the difference of various overlapped forms due to its convenience and immediacy. Lee et al. [7] estimated the joint strengths of overlaps, experimenting with various overlap lengths, forms, and thickness. Caiazzo et al. [8] adopted Seemann composite resin infusion molding process (SCRIMP) to manufacture test specimens, discussing the varying overlap properties and forecasting the fracture of lap joints. Do and Lee [9] used experimental methods to compare the tensile properties of normal model, overlapped model, and discontinuous model. The tensile properties were functions of the effective fiber volume fraction, and the differences of these functions were examined and used to predict the overlap-damage and discontinuous-damage parameters. Ma et al. [10] confirmed that structural failure of joints occurred in the adhesive layer or the bonded interface, and impact resistance of the joint increased as the overlap length increased. Gray et al. [11] conducted experiments and confirmed that laminate thickness has a significant effect on joint stiffness and ultimate load, both of which rise with increase in joint thickness.

In addition to experimental method, finite element method (FEM) and numerical simulations have been used to estimate the failure of overlap. Magalhães et al. [12] simulated composite bonded single-lap joints using two-dimensional FEM. The interface elements also considered to obtain stress field between different materials. This research results show important stresses variation along the adhesive thickness near the extremities of the overlap length. Panigrahi and Pradhan [13] and Panigrahi [14] adopted a 3D FEM model to simulate a single-lap joint and discuss the distribution of shear stress when it bears the out-plane loadings, and subsequently estimate the delamination strengths of single-lap joints. Das and Pasdhan [15] used FEM and Tasi–Wu failure criteria to simulate the failure properties of overlap. Yang [16] conducted experiments and numerical simulation to observe the tensile failure modes of single-lap joints. According to experimental results, Yang found that the joint strength was not linear with the adhered thickness and much affected by spew fillets in overlap ends. Furthermore, the simulation results showed that it is a main factor leading to joint failure when the maximum peel/shear stress occurred at overlap area edges and peel/shear stress of joint, with spew fillet at the overlap area edges less than that of joint with no spew fillet.

In addition to exploring the mechanical properties of overlap joints, the improvement of overlap forms are also being discussed. Castro and Keller [17] proposed a ductile adhesive joint design to enhance the bonding strength of FRP structures. Ductile

adhesive joint can develop a uniform stress distribution along the overlap length; thereby, enabling sufficient joint rotation to provide internal force redistribution that increases structural safety and robustness. Boseman et al. [18] modified the end shape of butt joint to determine its effect on interface strength, and confirmed that the butt joint can be stronger than the overlap joint regardless of loading types and directions.

In the current study, experiments and finite-element numerical simulations were conducted to explore the mechanical properties of various overlap forms and the failure strengths of joints. Ideal overlap forms for the use in laminated construction designs are suggested based on the findings.

2. Experiment method

Overlap modes are used in laminated FRP constructions to maintain fiber continuity. In addition to overlap, butt-joint connections can be used; thus, these connection methods were combined to manufacture the test samples in this study.

Experiments and numerical simulations were conducted to explore the mechanical properties of various overlap forms. The test specimens were manufactured according to the ISO-527-4 rule, and subsequently tensile tested to determine the varying fracture modes. An overlap length of 25 mm was considered. To avoid stresses from concentrating in specific overlap regions, the overlap regions and butt joints could not be located on the same cross sections.

Four stackings were used for each specimen. In accordance with the ISO-527-4 rule, the specimen size was 250 mm × 25 mm. The SCRIMP method was used to manufacture the specimens. The test specimens were fabricated using LT-800/M-225 and polyester resin-1629. The LT-800 fiber cloth provided orthotropic strength, and the mat M-225 provided bonding strength in each stacking layer. The volume fraction of the fiber was confirmed to be 61% using a combustion test and the single-layer thickness was 0.9 mm.

Based on various bonding styles, four types of overlap specimens were examined: (1) continuous fiber (CF) specimens. Each stacked CF layer is continuous; (2) FO specimens. FO is the common overlap form where each stacking layer comprises disconnected fibers that require overlap installations to facilitate linking. An overlap length of 25 mm was used herein; (3) FB specimens. The adjacent butt joints of each layer of FB specimen are separated by at least 25 mm, and butt joints are 37.5 mm away from the clamp ends; and (4) OOAIB specimens. In an OOAIB situation, the disconnected fibers in the top and bottom layers are connected using overlap installation and the disconnected fibers in the two inner layers are connected using butts. The adjacent butt

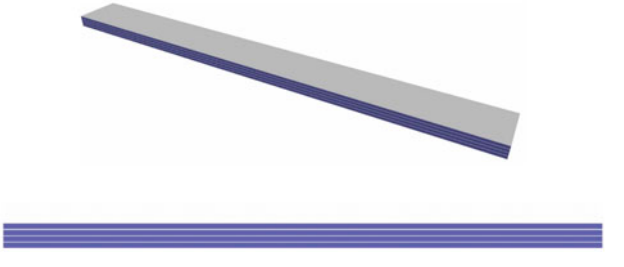

Figure 1. CF specimen.

joints in the two inner layers are separated by 50 mm. Figure 1 shows the CF specimen shape. Figures 2–4 show the specimen shapes and discontinuous locations of FO, FB, and OOAIB specimens individually.

An HT-9102 material testing machine was used to conduct tensile testing, using SF-014D wedge grip and HT-9160 extensometer set. The results showed that the wedge grip exhibited insufficient clamp ability. A slip existed between the wedge grip and specimens, but this slip disappeared when the tensile length was approximately 2 mm. The boundary slip was absent in simulation. Therefore, the INSTRON-5582 material

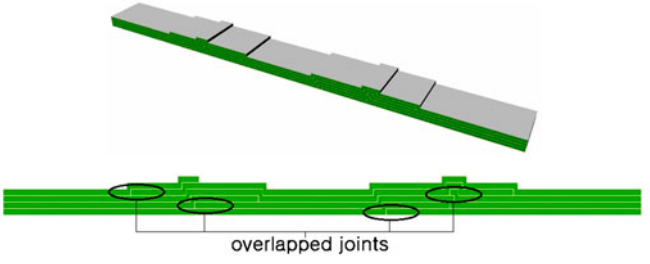

Figure 2. FO specimen.

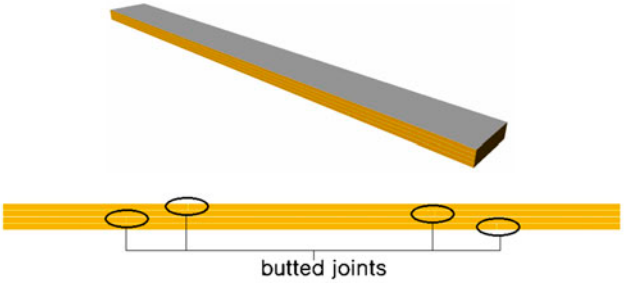

Figure 3. FB specimen.

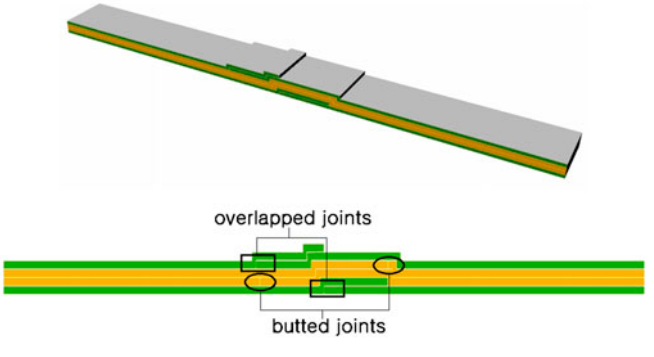

Figure 4. OOAIB specimen.

Table 1. Material properties.

	Young modulus (MPa)	Poisson ratio $v_{12} = v_{21}$	Breaking strength (MPa)	Breaking strain (%)	Shear modulus (MPa)	Shear strength (MPa)	Density (g/cm^3)
Polyester	3550	0.38	55	1.8	1350	50	1.2
E-Glass	73,100	0.238	2750	3.8	30,000	1700	2.57
LT-800/M-225 (W_f = 61%)	20,500	0.143	380	1.8	3330	–	–

testing machine was chosen using the spiral grip to improve the boundary slip. Finally, the experiment results obtained by INSTRON-5582 will be the basis for comparison with simulation results.

3. Numerical simulation assumptions

In this study, the finite element ANSYS package was used to simulate the in-plane strength of overlap regions. The stacking layers were constructed using solid elements. Furthermore, the layered orthotropic material parameters of each direction were investigated using classical laminated plate theory.

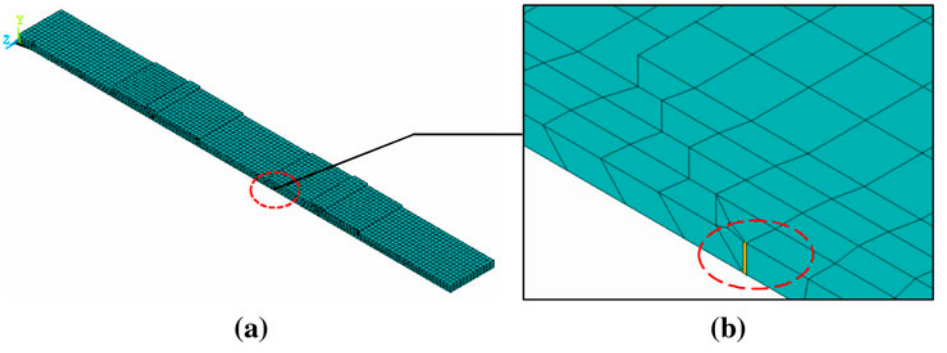

Figure 5. FEM model of FO specimen.

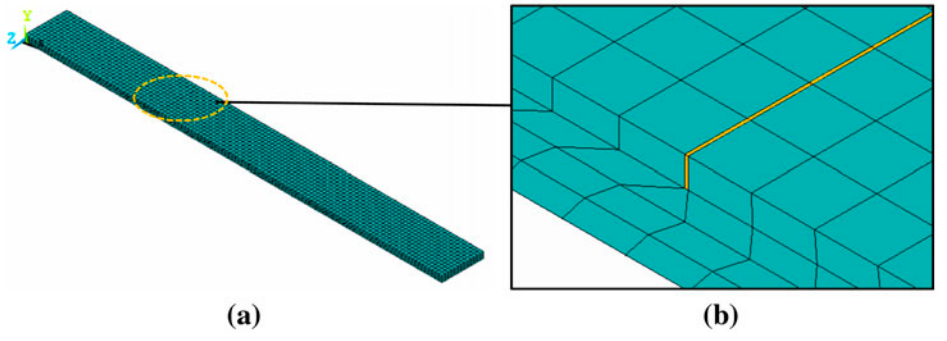

Figure 6. FEM model of FB specimen.

Table 2. HT-experiment results – CF.

	CF			
No.	$Width_{average}$ (mm)	$Thickness_{average}$ (mm)	Pmax (N)	Strength (N/mm^2)
1	24.32	4.04	36401.121	370.5351
2	24.52	3.93	36489.321	378.7144
3	24.62	3.85	33462.100	353.2822
4	24.47	3.98	33140.660	340.0476
5	24.77	3.92	33501.300	345.3643
6	24.58	3.98	36527.540	373.0208
Average	24.546	3.95	34920.340	360.16
Standard deviation	0.152	0.067	1705.574	16.05
Coef. of variation	0.62%	1.7%	4.88%	4.46%

Table 3. HT-experiment results – FO.

	FO			
No.	$Width_{average}$ (mm)	$Thickness_{average}$ (mm)	Pmax (N)	Strength (N/mm^2)
1	24.83	4.050	20348.721	202.3918
2	24.80	3.940	21889.281	224.0183
3	24.82	3.995	26201.281	264.2433
4	24.75	3.825	23037.840	243.3521
5	24.75	3.975	21841.260	222.0063
6	24.80	3.875	24439.240	254.3618
Average	24.79	3.94	22959.64	235.06
Standard deviation	0.033	0.082	2903.65	23.03
Coef. of variation	0.13%	2.08%	9.12%	9.8%

Table 4. HT-experiment results – FB.

	FB			
No.	$Width_{average}$ (mm)	$Thickness_{average}$ (mm)	Pmax (N)	Strength (N/mm^2)
1	24.88	3.925	15518.300	158.9430
2	24.78	3.980	14820.540	150.3029
3	24.83	3.825	15420.300	162.3948
4	24.75	3.975	15226.261	154.7679
5	24.68	3.650	13909.140	154.4366
6	24.58	3.750	14450.100	156.8000
Average	24.746	3.851	14890.774	156.2742
Standard deviation	0.108	0.133	624.415	4.1512
Coef. of variation	0.44%	3.46%	4.19%	2.66%

LT-800 and M-225 were arranged with unsaturated polyester resin to fabricate the test specimens. The oriented fiber of LT-800/M-225 is E-glass; the Young's modulus of E-glass is 73.1 GPa, where the shear modulus is 30 GPa and the fracture strength can attain 2.75 GPa. Furthermore, the Young's modulus of unsaturated polyester resin is 3550 MPa, shear modulus is 1350 MPa, and fracture strength is 55 MPa.

Table 5. HT-experiment results – OOAIB.

	OOAIB			
No.	$Width_{average}$ (mm)	$Thickness_{average}$ (mm)	Pmax (N)	Strength (N/mm^2)
1	24.90	3.875	20466.321	212.1137
2	24.98	3.850	20999.440	218.3944
3	24.93	3.850	19819.520	206.5367
4	24.93	3.920	16994.180	173.9318
5	25.00	3.925	17045.140	180.6347
6	25.00	3.825	21143.500	221.1527
Average	24.953	3.874	19411.350	202.1273
Standard deviation	0.042	0.041	1910.162	21.6351
Coef. of variation	0.17%	1.05%	9.84%	9.90%

Table 6. INS-experiment results – CF.

	CF			
No.	$Width_{average}$ (mm)	$Thickness_{average}$ (mm)	Pmax (N)	Strength (N/mm^2)
1	24.410	3.880	34115.860	360.2100
2	24.480	4.030	29881.500	302.8900
3	24.560	3.930	32710.310	338.8900
4	24.670	3.830	36168.690	382.7900
5	24.480	4.050	32517.380	327.9800
Average	24.520	3.944	33078.748	342.55
Standard deviation	0.099	0.095	2307.413	30.5358
Coef. of variation	0.40%	2.40%	6.98%	8.91%

Table 7. INS-experiment results – FO.

	FO			
No.	$Width_{average}$ (mm)	$Thickness_{average}$ (mm)	Pmax (N)	Strength (N/mm^2)
1	24.980	3.830	23185.570	242.3400
2	25.030	3.840	23976.840	249.4600
3	24.790	4.050	26243.860	261.3900
4	24.800	4.060	23202.660	230.4400
5	24.780	3.980	26924.120	273.0000
Average	24.876	3.952	24706.610	251.3260
Standard deviation	0.119	0.111	1759.864	16.5189
Coef. of variation	0.48%	2.81%	7.12%	6.57%

LT-800 is an orthotropic material and M-225 is a quasi-isotropic material. Combining LT-800 and M-225 generates a new orthotropic material. Furthermore, the fiber weight fraction $W_f = 61\%$ was determined using a combustion test. When the volume fraction is known, the orthotropic parameters of LT-800/M-225 can employ classical laminated plate theory to obtain. Because LT-800/M-225 is an orthotropic material, the in-plane moduli E_x and E_y can be treated the same and considered to be

Table 8. INS-experiment results – FB.

	FB			
No.	$Width_{average}$ (mm)	$Thickness_{average}$ (mm)	Pmax (N)	Strength (N/mm^2)
1	24.820	3.990	17661.950	178.3500
2	24.830	3.990	17478.380	176.4200
3	24.780	3.920	17813.820	183.3900
4	24.840	4.230	15970.820	152.0000
5	24.830	3.950	16473.010	167.9600
Average	24.820	4.016	17079.596	171.62
Standard deviation	0.023	0.123	811.57	12.3005
Coef. of variation	0.09%	3.07%	4.75%	7.17%

Table 9. INS-experiment results – OOAIB.

	OOAIB			
No.	$Width_{average}$ (mm)	$Thickness_{average}$ (mm)	Pmax (N)	Strength (N/mm^2)
1	24.980	4.070	19779.940	194.5500
2	25.000	3.930	20399.830	207.6300
3	24.980	3.830	18757.390	196.0600
4	24.940	3.800	20280.370	213.9900
5	24.850	4.030	19658.400	196.3000
Average	24.950	3.932	19775.186	201.7060
Standard deviation	0.060	0.119	650.953	8.6357
Coef. of variation	0.24%	3.02%	3.29%	4.28%

20.5 GPa. In addition, the out-plane strength is controlled using resin, and the out-plane modulus E_z can be considered approximately the same as the resin. Table 1 lists the detailed material parameters of LT-800 and M-225.

Concerning the arrangement of the finite element model, the 3D solid element program, Solid-185, was used to establish a laminated plate model. The large deformation, geometric, and material nonlinearity calculations were all supported using Solid-185. Figure 5 presents the FEM model of FO. To simulate the fiber discontinuity in the overlap region, a gap of resin was necessary to seclude the fibers in the identical layer. The gap of resin assumed in this study is 0.1 mm. Figure 5(b) presents the local fiber discontinuity model of FO. The circular mark indicates the seam of the resin. The 0.1 mm seam of resin was adopted to separate each continuous layer of FO specimen.

The fiber discontinuity was similarly treated in the butted-joint model and overlap models, where the seam of the butt zone was arranged using 0.1 mm of filler resin to simulate the fiber discontinuity. Actually, this assumption of model arrangement agreed well with the realistic stacking situation. Figure 6(a) presents the FEM model of FB; the yellow elements marked in Figure 6(b) indicate one of the seams of the butt zone.

A linear simulation was first conducted to determine the specimen rigidity, and confirms that the rigidity results of the experiment and simulation corresponded. Subsequently, the fracture strength was examined through simulation. ANSYS includes a bilinear elasticity analysis feature for simulating material failure. If the local stress in

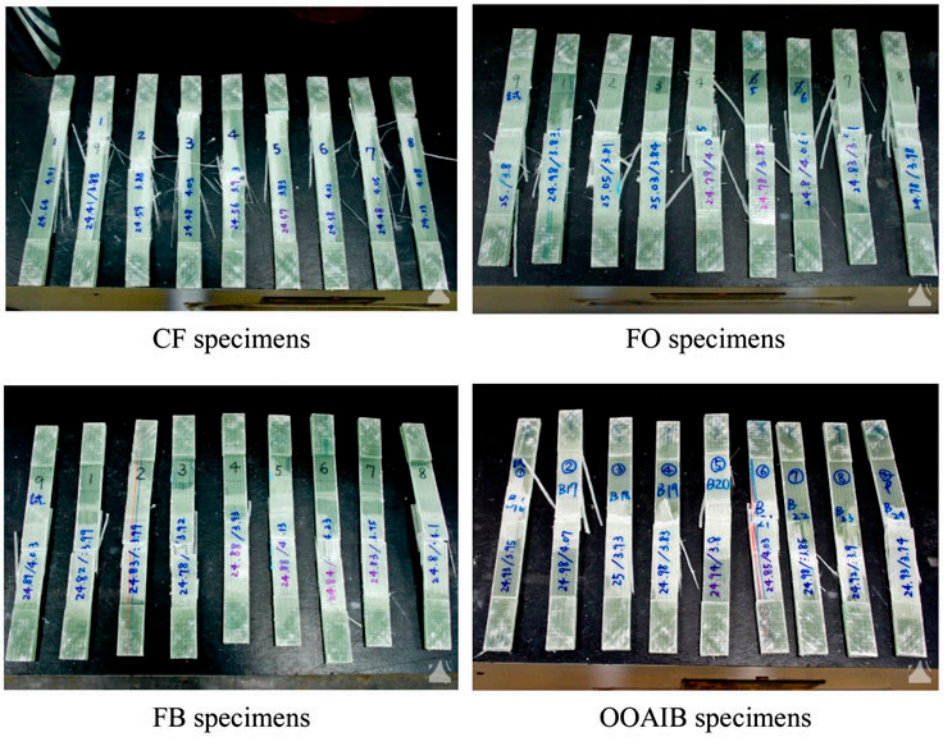

Figure 7. Fracture modes on the even side.

an overlap region reaches fracture stress, this bilinear elastic relation can automatically modify the rigidity of the local element to simulate the correspondingly decreased rigidity. In this study, the supposed modify rigidity was 1% of the initial rigidity.

4. Discussion

4.1. Experiment results

At least nine specimens per group underwent tensile testing; the specimens that exhibited lower and unreasonable resistance were removed to facilitate analyzing and comparing the remaining specimens. Tables 2–9 list the summarized results. Tables 2–5 list the experimental results recorded using the HT-9102 machine and Tables 6–9 lists the experimental results recorded using the INS-5582 machine.

The existing overlap causes uneven thickness distribution. Furthermore, the test specimens were fabricated on an even plate; thus, the overlapping region on the other side caused asymmetrical specimens. The tensile test results indicated that the loading resistance was weaker on the even side compared with the overlapping side. During the experiment, the even sides of each specimen almost broke entirely.

Tensile testing indicated that the fractures among the CF specimens always occurred near the constrained ends because the stacking layer in the tensile region comprised CFs, and the loading transference was smooth. The constrained ends exhibited clear geometric discontinuities; thus, they really produced concentrated stress. The fracture modes of the other specimens occurred at discontinuous fiber locations. The OOAIB

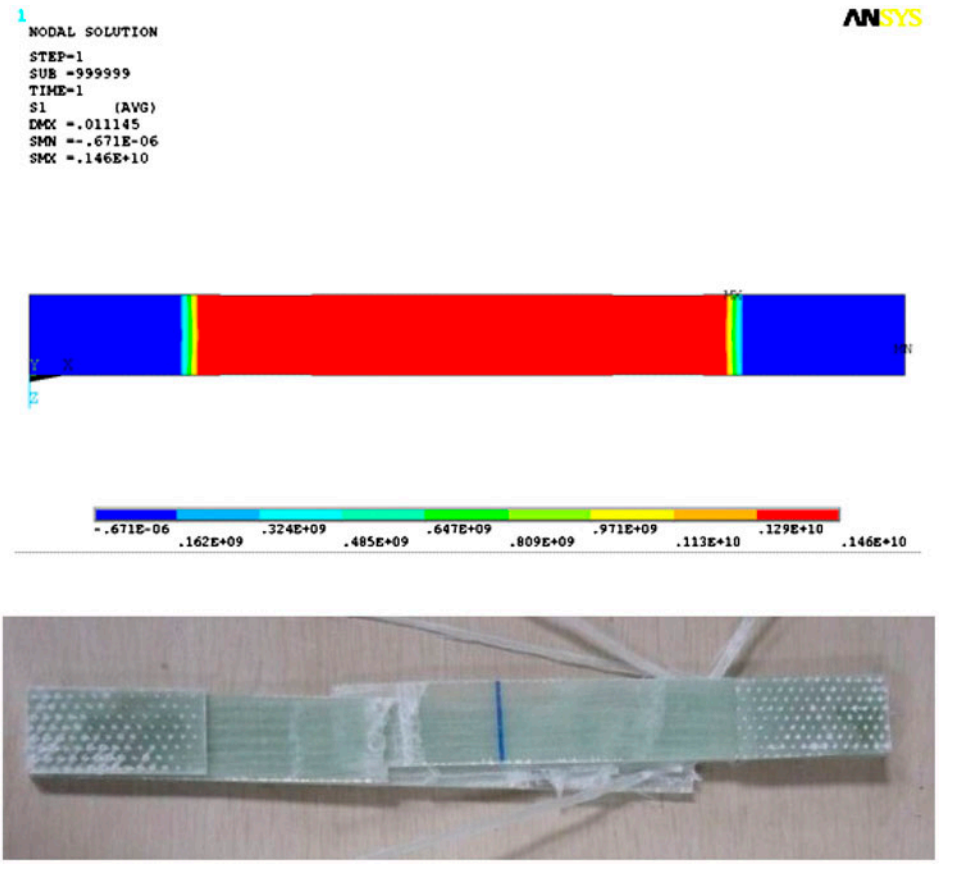

Figure 8. Fracture modes compared with experimental and simulation results – CF.

specimens fractured at the butted-joint layers, the FO specimens fractured on the even side and the FB specimens were nearly entirely broken at butt joints of each stacking layer. Figure 7 demonstrates the even side fracture modes of specimens that exhibited various overlapping style.

The summarized experimental results indicated that the CF series endured maximal loading; the tensile resistance of the FO series was weaker compared with the CF series, and the tensile resistance of the FB series was the weakest. The strength resistance of OOAIB series was approximately 85% compared with the FO series; however, comparing the weights of overlap regions indicated that the OOAIB series was approximately 50% less heavy than the FO series was. If the stacking number increases, weight economy is expected.

When constructing an FRP yacht, the overlap location of each stacking layer is approximately dispersed to avoid stress concentration. The tensile test specimens examined in this study were limited by the ISO rules and the close joint region may cause the underestimation of tensile strength. If the overlap or butt region can be approximately dispersed, the strength of the OOAIB model can be increased similarly to that of the FO model.

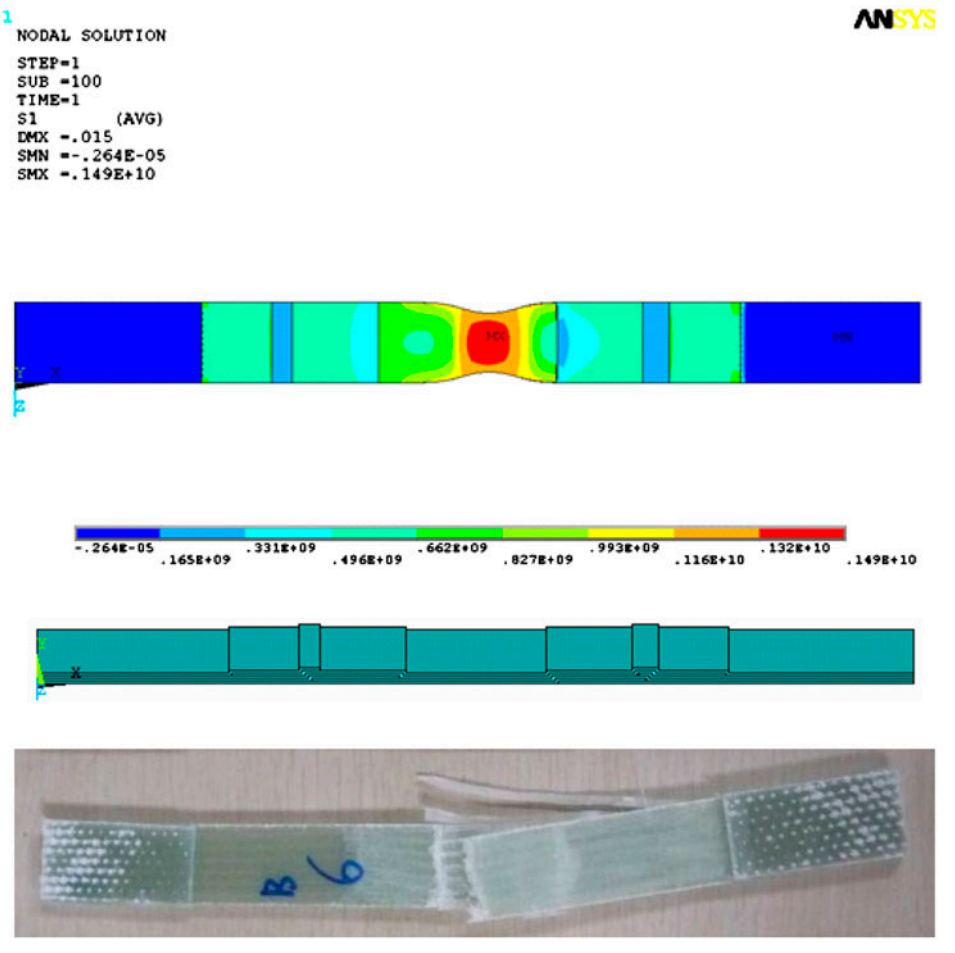

Figure 9. Fracture modes compared with experimental and simulation results – FO.

The HT-9120 and INS-5582 material testing machines were used, employing various clamping mechanisms to perform tensile tests. During the test process, the wedge grip of the HT-9120 machine generated clamp sliding between the grip and test specimens; however, the spiral grip of the INS-5582 machine tightly constrained the test specimens. Comparison of the results indicated that both machines yielded similar rigidity and tensile values. If the clamp sliding is neglected, the fracture strength and rigidity results of both machines can be viewed as identical. The experimental and ANSYS simulation results are compared and discussed in the subsequent paragraph.

4.2. *Numerical simulation results*

Figures 8–11 compare the simulated and experimental results regarding the fracture locations. Concerning the CF case, because the stacking layers comprised CFs and lacked butted-joint or overlap regions, the stress concentration fracture was able to occur at any position.

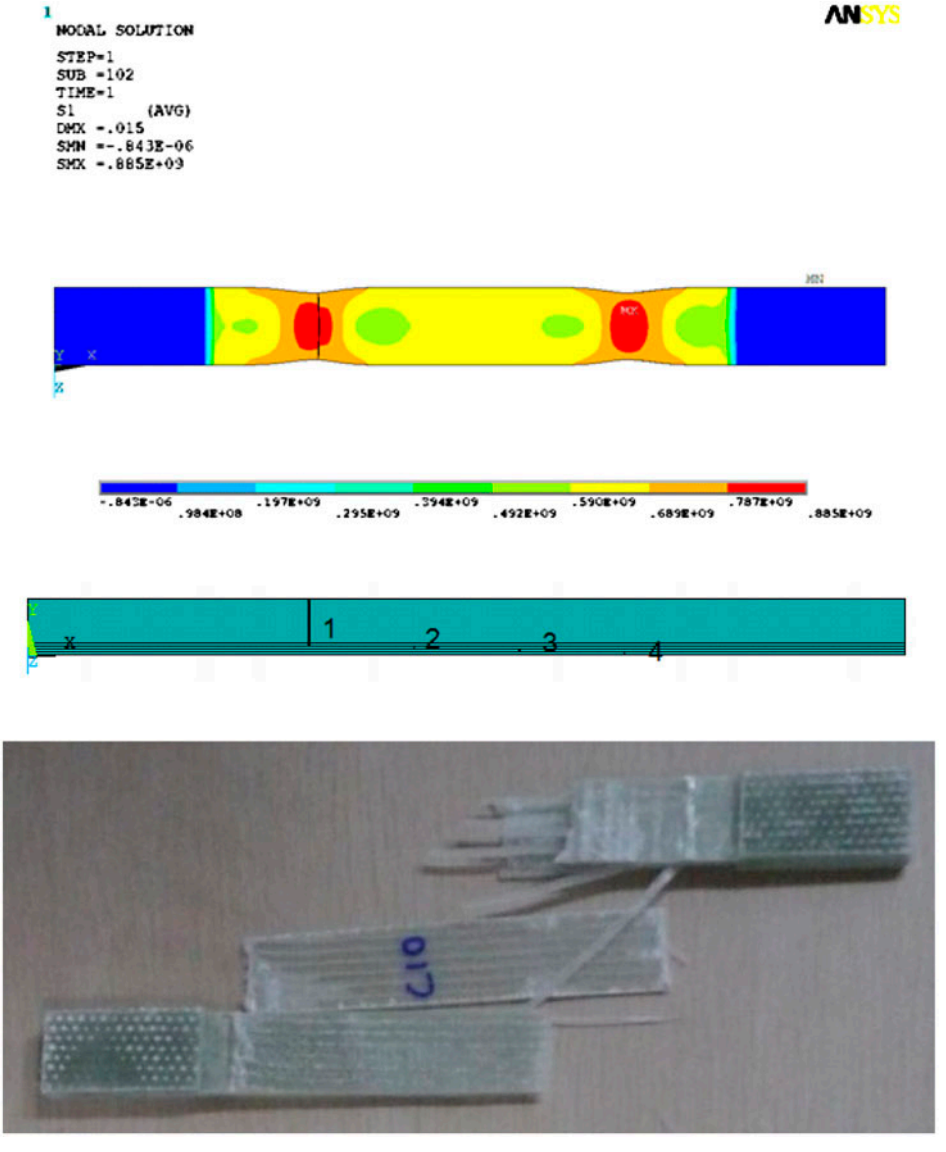

Figure 10. Fracture modes compared with experimental and simulation results – FB.

Figure 9 compares the simulated and experimental results of the FO specimens. The overlap regions of the FO specimens were located at one-fourth and three-fourths of its length, and the middles of the specimens were the thinnest locations. Thus, the overlap region endured the tensile loading and the tensile resistance was stronger at the overlap region compared with the CFs in the middle region.

Figure 10 compares the simulated and experimental results of the FB specimens, among which the butt joint regions were evenly dispersed. According to these results, fractures readily occurred at the butt joint near the constrained ends. Moreover,

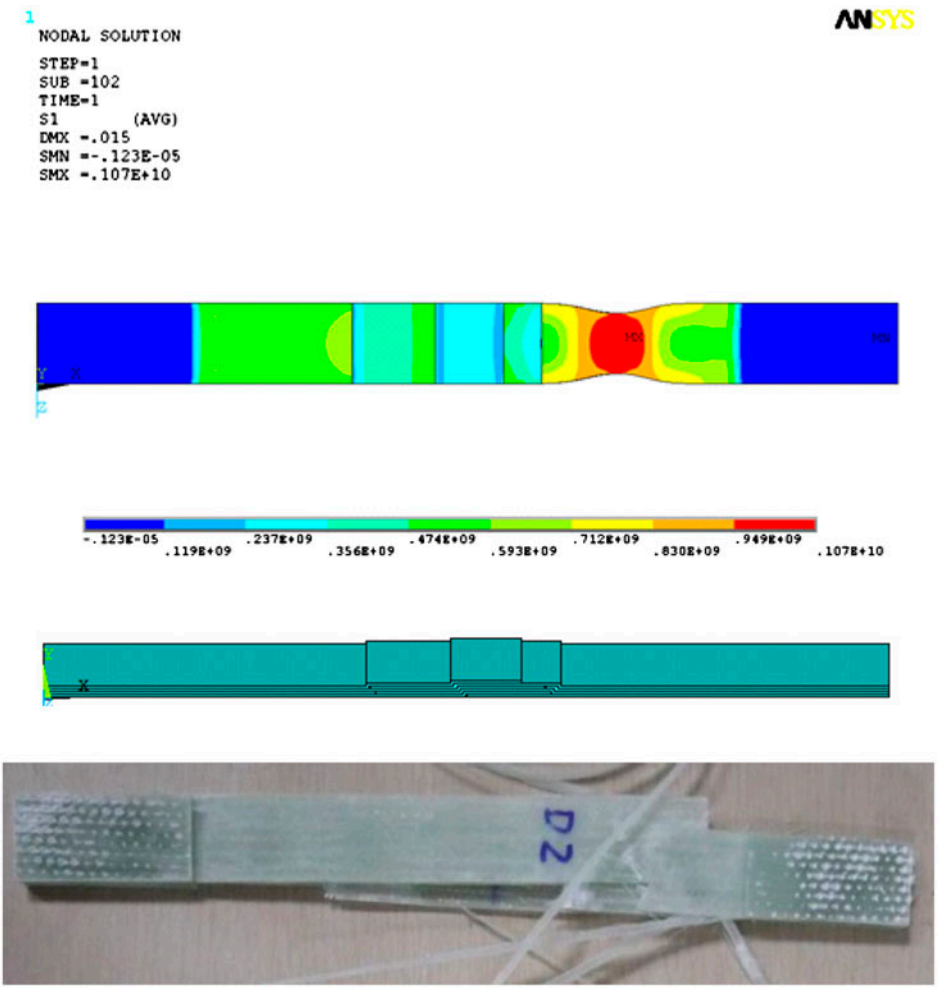

Figure 11. Fracture modes compared with experimental and simulation results – OOAIB.

fractures always occurred first at the butt joint at the surface layer, always accompanying delamination between the surface and second layers. In summary, the complete fracture of FB specimens always involved fiber fracture and delamination.

Figure 11 compares the experimental and simulated results of OOAIB testing. The overlap and butted-joint regions of the OOAIB specimens were located at the center of its length, and the middles of specimens were the thickest locations. The primary fracture occurred on the even side and located at one-fourth or three-fourth of its length. With the increase in stress concentration, the secondary fracture occurred at the butted-joint accompanied.

Figures 12–15 show the relation between loading and displacement. The tensile test data were recorded using the INS-5582 and HT-9120 testing machines. 'ANSYS_L' (Figures 12–15) indicates the linear simulation results and 'ANSYS_NL' indicates the nonlinear simulation results in which the fracture strength was considered. Because of

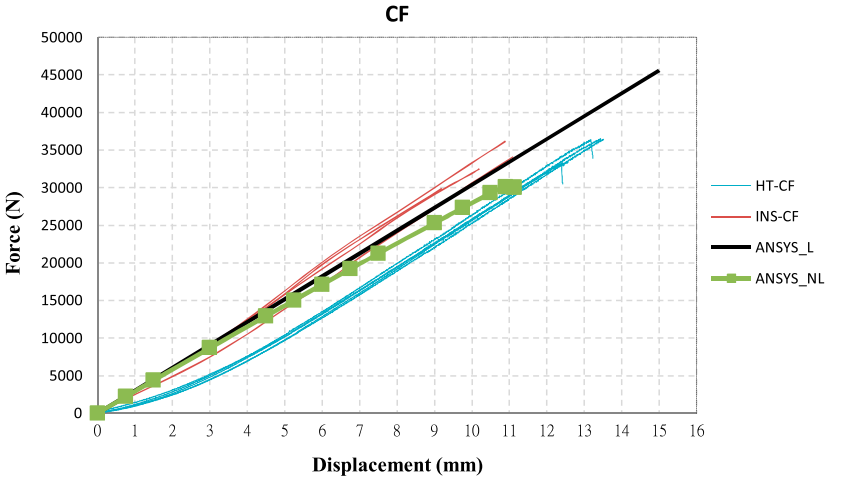

Figure 12. Comparison of experimental and simulation results – CF.

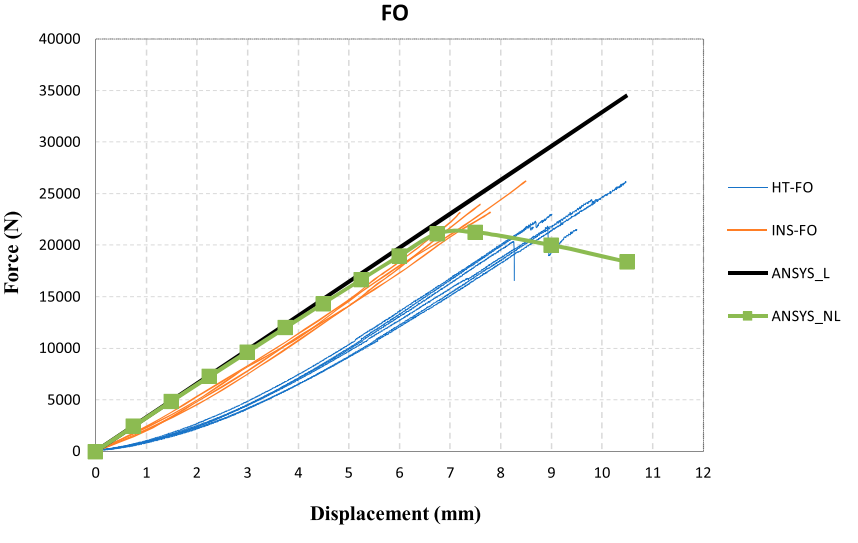

Figure 13. Comparison of experimental and simulation results – FO.

the slip existed between the wedge grip and specimen, the initial rigidity of HT series was lesser than INS series. With the increase in tensile loading, the rigidities of HT and INS series were approximated gradually. The simulation method used in this study is mainly compared with the INS experiment results.

In summary, the simulated and experimental results were similar, confirming the accuracy of the simulation method used in this study.

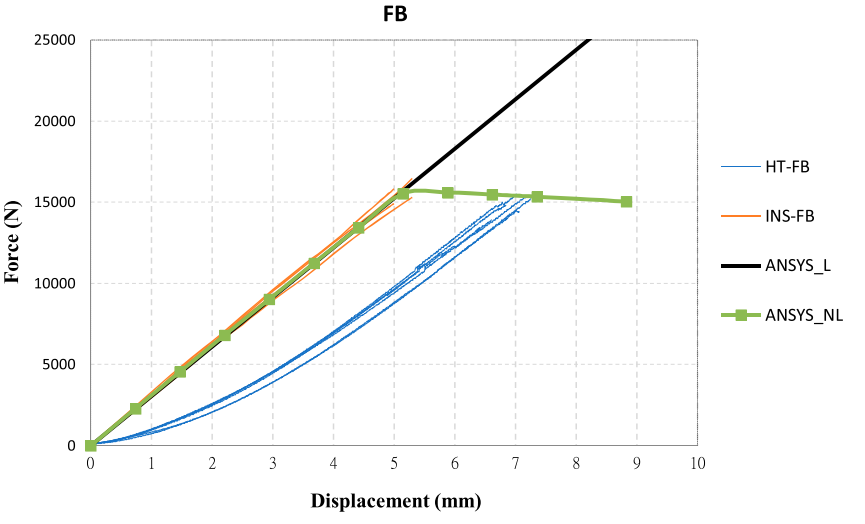

Figure 14. Comparison of experimental and simulation results – FB.

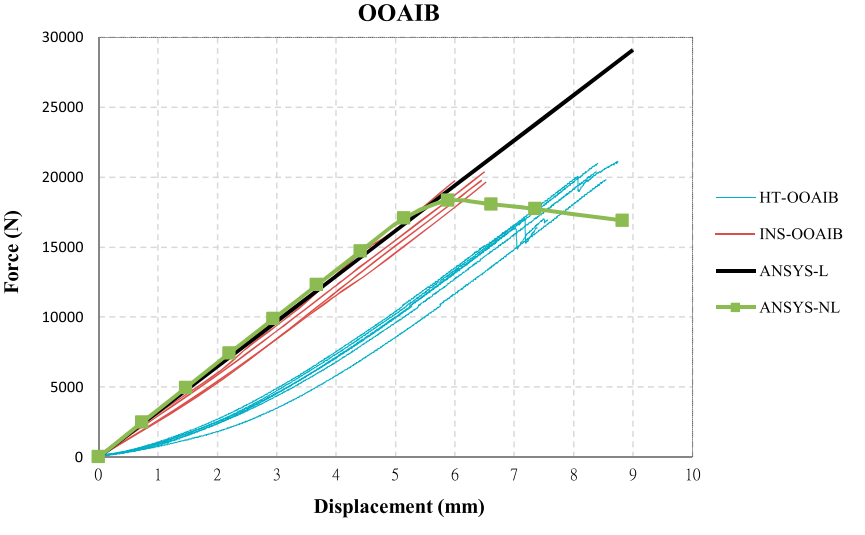

Figure 15. Comparison of experimental and simulation results – OOAIB.

5. Conclusions

In this study, ANSYS was used to simulate the tensile strengths and fracture modes. The layer discontinuity models and failure rigidity modifications were considered to observe the fracture properties of various overlap forms. Then, the simulated and experimental results were compared to verify the accuracy of the proposed method, verifying that numerical simulation can be applied to simulate the fracture properties of various overlap forms.

'FO' is the most common overlap form. However, FO involves overlap regions in each stacking layer, yielding excessive weight among laminated constructions. The

enhanced OOAIB overlap form suggested in this study was proposed to reform the shortcomings of the FO method. The findings indicated that the tensile strength of OOAIB is approximately 85% compared with that of FO; however, OOAIB demonstrates a decreased weight of approximately 50% in the overlap regions. Thus, the proposed design facilitates the lightweight design of laminated constructions.

Acknowledgment

The authors would like to thank the National Science Council of the Republic of China for financially supporting this research.

References

[1] Beylergil B, Aktas A, Cunedioglu Y. Buckling and compressive failure of stepped-lap joints repaired with composite patches. J. Compos. Mater. 2012;46:3213–3230.
[2] Langella A, Carbone R, Nele L, Rosolia M. An analytical closed-form model to evaluate the peel and shear stresses in middle plane for adhesively bonded composite single-lap joints. J. Compos. Mater. 2012;46:3–17.
[3] Adriana WB, Lopes CS, Kromwijk PJ, Gurdal Z, Camanho PP. A theoretical model to study the influence of tow-drop areas on the stiffness and strength of variable-stiffness laminates. J. Compos. Mater. 2009;43:403–425.
[4] Delale F, Erdogan F, Aydinoglu MN. Stresses in adhesively bonded joints: a closed-form solution. J. Compos. Mater. 1981;15:249–271.
[5] Adkins DW. Strength and mechanics of bonded scarf joints for repair of composite materials [Ph.D. thesis]. University of Delaware; 1982.
[6] Agarwal BD, Broutman LJ. Analysis and performance of fiber composites. Hoboken, NJ: John Wiley; 2006.
[7] Lee HK, Pyo SH, Kim BR. On joint strengths, peel stresses and failure modes in adhesively bonded double-strap and supported single-lap GFRP joints. Compos. Struct. 2009;87:44–54.
[8] Caiazzo A, Bonanni D, Telegadas H. Parametric testing of scarf joints for Navy composite structures. In: International SAMPE Technical Conference, Long Beach, CA; 2004. p. 1831–1843.
[9] Do TT, Lee DJ. Degradation in tensile properties with overlapped and discontinuous fabric preforms. Adv. Compos. Mater. 2011;20:443–462.
[10] Ma Y, Zhang K, Yang Z, Li Y. Effects of impact om the failure of CFRP/Al bonded single-lap joints with different overlap length. Adv. Mater. Res. 2011;181–182:814–819.
[11] Gray PJ, O'Higgins RM, McCarthy CT. Effects of laminate thickness, tapering and missing fasteners on the mechanical behaviour of single-lap, multi-bolt, countersunk composite joints. Compos. Struct. 2014;107:219–230.
[12] Magalhães AG, de Moura MFSF, Gonçalves JPM. Evaluation of stress concentration effects in single-lap bonded joints of laminate composite materials. Int. J. Adhesion Adhesives. 2005;25:313–319.
[13] Panigrahi SK, Pradhan B. Delamination damage analyses of adhesively bonded lap shear joints in laminated FRP composites. Int. J. Fracture. 2007;148:373–385.
[14] Panigrahi SK. Damage analyses of adhesively bonded single lap joints due to delaminated FRP composite adherends. Appl. Compos. Mater. 2009;16:211–223.
[15] Das RR, Pradhan B. Adhesion failure analyses of bonded tubular single lap joints in laminated fibre reinforced plastic composites. Int. J. Adhesion Adhesives. 2010;30:425–438.
[16] Yang Y. Failure analysis of laminates single-lap adhesive joints under uniaxial tensile loading. Adv. Mater. Res. 2012;490–495:2201–2204.
[17] Castro Julia, Keller T. Design of robust and ductile FRP structures incorporating ductile adhesive joints. Compos. Part B: Eng. 2010;41:148–156.
[18] Boseman MF, Kwon YW, Loup DC, Rasmussen EA. Interface fracture of hybrid joint of glass-/steel-fiber composite. Eng. Comput. 2012;29:504–527.